HiSST: 3rd International Conference on
High-Speed Vehicle Science Technology
14 -19 April 2024, Busan, Korea

Simulation of the mixing of a supersonic air flow with a transverse jet under the conditions of pulse-periodic local heating

Aleksandr A. Firsov[1], Luka S. Volkov[2], Yakov V. Miroshnikov[2]

Abstract

When a supersonic air flow interacts with a transverse secondary jet injected into this flow through an orifice on a flat wall, a special flow structure is formed. This kind of flow has set of technical applications related to fuel combustion; therefore, various approaches to intensifying gas mixing in this type of flow are proposed and studied. This work is devoted to the approach which implies using electric discharges for pulsed heating of the medium and generating the instabilities in the shear layer at the boundary of the secondary jet. In the software package FlowVision the characteristics of the flow are simulated in the absence and presence of pulsed-periodic local heating on the injector windward side. The calculations are performed for three jet-to-crossflow momentum flux ratios: 0.7, 1.0 and 1.3. Six modes of pulse heating are investigated: they have different frequencies of pulsed heating (from 10 to 60 kHz), but they have the uniform average power release. This work demonstrates that pulsed heating can stimulate the formation of perturbations in the shear layer at the jet boundary and can lead both to a decrease in the average mixing efficiency and to its increase (up to 15%). The optimal frequencies of the pulsed heating are found.

Keywords: *CFD, spark discharge, transverse injection, FlowVision, URANS*

Nomenclature

Latin

D – diameter of the jet orifice
F – frequency of pulsed heating
M – Mach number in the freestream
NS – Navier-Stokes equations
J – jet to-crossflow momentum flux ratio
JISC – jet interacting with supersonic crossflow
LDV – laser Doppler velocimetry
LES – large eddy simulation
P – static pressure
P_t – total pressure
RANS – Reynolds-averaged NS
CFD – Computational Fluid Dynamics
Sr – Strouhal number
SST – Shear Stress Transport
T – static temperature
T_t – total temperature
Q_m – mass flow in the secondary jet
U – local velocity
URANS – unsteady RANS
W – local mass fraction of CO_2
Z^+, Z^- – boundaries of computational domain at maximum and minimum Z coordinate

Greek

η_m – mixing efficiency (an integral criterion)
ρ – local density
τ – duration of one heating pulse

Subscripts

jet – corresponding to the secondary jet
∞ – corresponding to the freestream

[1] *JIHT RAS, 125412, Izhorskaya st. 13 Bd.2, Moscow, Russia, af@jiht.org*
[2] *JIHT RAS, 125412, Izhorskaya st. 13 Bd.2, Moscow, Russia*

1. Introduction

In recent decades studies have been performed in several countries [1, 2] in order to develop new solutions for a number of scientific and engineering problems related to the intensification of gas mixing and combustion in subsonic and supersonic flow. These studies may be applicable, as an example, for raising the efficiency of scramjet combustion chambers with a supersonic flow at the inlet [3] by intensifying the mixing of a fuel with an oxidizer (air).

The following recent works demonstrate some actual aspects of the problems of mixing and combustion in supersonic flow. The paper [4] demonstrates that the liquid injection exhibits similar mixing efficiency in the cavity compared to the gaseous injection with the same equivalent ratio. Diagnostic methods in [4] are high-speed photography and pressure scanning. In [5] the effects of the primary rocket's excess oxidizer coefficient on the performance of a kerosene-fueled rocket-based combined cycle engine are investigated numerically (RANS with SST). Complete mixing and chemical equilibrium assumptions are employed.

In the work [6] the authors numerically investigate the mixing of air with ethylene and combustion in a chamber with a cavity flameholder. The 3D RANS simulation shows that with the increase of the separation zone the intensity of combustion in the reacting flow field is also increased. The work [7] elucidates the numerical investigation of the mixing and combustion processes of a kerosene jet injected into a scramjet combustor with dual-cavity at different global fuel equivalence ratios. A hybrid RANS-LES numerical method and Yoshizawa sub-grid scale model is adopted. The work [8] reports about an experimental investigation of the influence of the backward-facing step and injection schemes on the spray characteristics of a liquid jet. Diagnostic methods applied in the work are high-speed photography and schlieren techniques.

In the abovementioned works the problem of supersonic combustion is closely connected with the problem of mixing. It indicates the actuality of the research aimed at developing new strategies for mixing intensification, involving both experimental and computational methods.

Since influencing on the mixing rate at the molecular scale seems to be difficult, one of the main approaches to the mixing intensification is increasing the boundary surface area of the secondary jet. One of the currently developing strategies involves pulse-periodic energy release in the area of mixing by means of electric discharges [9].

Our work is devoted to the computer simulation of the disturbances excited by electric discharges in the shear layer on the jet boundary in the JISC flow configuration and their role in the mixing intensification. The local characteristics of JISC flow are calculated in the absence and presence of repetitive spark discharge located at the windward edge of the injector orifice. The spark discharges are modeled as a periodic local heat source. This work elucidates a parametric study in which the optimal modes of spark discharge are chosen. The examined modes differ in the frequency of discharges and the energy released in one discharge, but the average power deposited in the discharges is uniform for all the cases.

This work is a continuation and development of the research in the direction outlined in the article [9]. The simulation is carried out as a preparation for future experiments in which an attempt will be made to induce instability in the JISC flow using plasma of periodic spark discharges.

2. Methods and CFD problems

2.1. Model and Validation

The 3D CFD modeling was performed using software package FlowVision. The program solved the URANS system by the finite volume method. The system of equations was supplemented by a modified k-ε turbulence model — KEFV [10]. This is one of the standard FlowVision turbulence models which performs well in simulating flow separation and reattachment flows.

The URANS method is currently uncommon for the simulations of JISC. Therefore, we validated the applied computer model using a particular JISC case, which had previously been investigated by different researchers from a number of countries: by both experimental and numeric methods (LDV [11], LES [12], RANS [13]). This case was reproduced in FlowVision. Fig. 1 shows the distribution of

Mach number in a symmetry plane, the grid and an example of a velocity profile with the comparison to the data of other researchers.

For the results obtained in FlowVision the grid convergence and satisfactory agreement to the data from other works were shown [9]. This similarity is an argument in favor of the applicability of the used computational model for JISC flows.

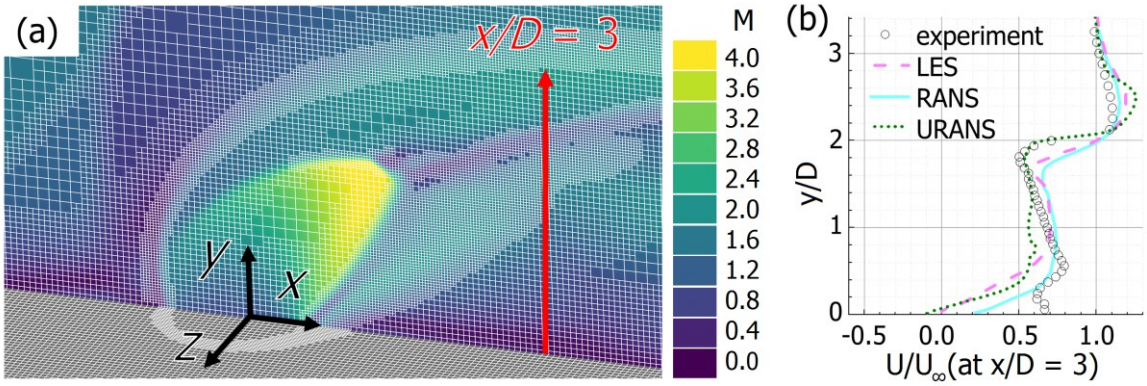

Fig 1. The case for the method validation. Distribution of averaged Mach number in the symmetry plane and the computational grid with adaptations (a), normalized profiles of the velocity x-component at the axis x/D = 3: comparison of our data (URANS) with the data obtained by other researchers by different methods (b): LDV (experiment) [11], LES [12], RANS [13]

2.2. Selection of the model plate shape and position in a wind tunnel

In the planned experiment for which the presented calculation is performed, gas injection will be carried out not directly from the wall of the wind tunnel channel, but from a special plate that cuts the core of the supersonic air flow in this tunnel. We expect that this modification will eliminate the influence of the turbulent boundary layer on the phenomenon under study in the experiments.

For clarity, Fig. 2 shows an example of an auxiliary 2D calculation that was performed using FlowVision. The flow around a plate with a sharp leading edge was obtained from this calculation. According to the calculation, the injection of a secondary jet through an orifice on the upper surface of the plate can significantly reduce the thickness of the boundary layer on the injection surface.

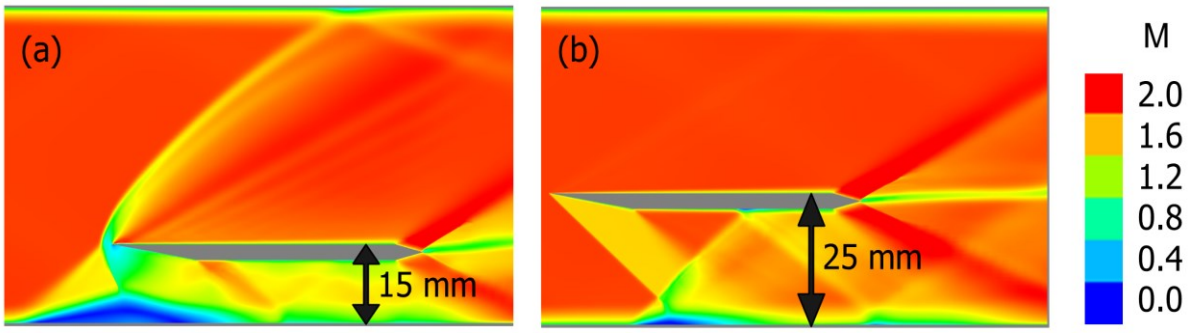

Fig 2. Two-dimensional modelling of supersonic flow around a flat plate in a wind tunnel. Unsuitable configuration, in which the flow over the plate is highly inhomogeneous (a); suitable configuration (b)

When proceeding from 2D to 3D calculations, it is necessary to take into account the influence of the walls Z^+, Z^- and the injector tube, which worsens the streamlining of the model and brings the flow field closer to case (a) in Fig. 2. The most actual version of the geometric configuration of the plate with which the experiment is being carried out is demonstrated in Fig. 3. It is provided with a slight (~5°) inclination of the injection plane (Fig. 3 a). This leads to a slight decrease in the Mach number above the injection plane (Fig. 3 b), but provides a uniform air flow above the injection plane without the formation of extensive subsonic zones. In this work, in the following calculations we neglect the correction to the Mach number in a supersonic air flow and round it to 2 as it is in the freestream.

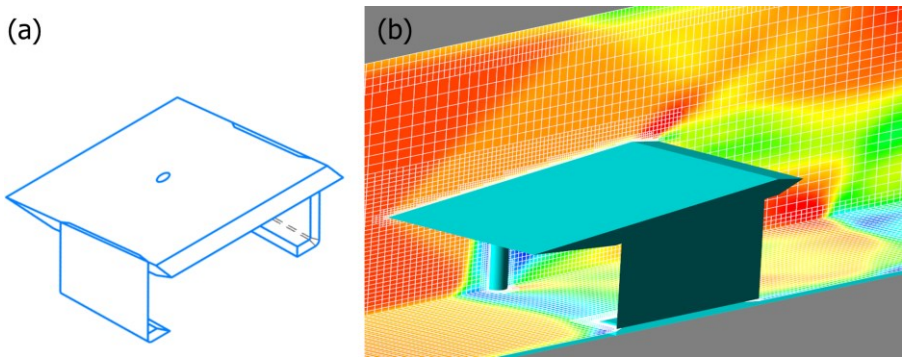

Fig 3. 3D model (a) of a plate manufactured for injection of a secondary jet into a supersonic air flow in a wind tunnel channel. Calculation of supersonic flow around the model (b)

2.3. Boundary conditions and grid

The computational domain for the cases under study is shown in Fig. 4. For ease of perception, a symmetrical area is shown. However, only the half-space Z > 0, limited by the dotted line Z = 0, was simulated in our calculations. Callouts in Fig. 4 shows the location of the area of a spark discharge and an example of a computational grid with adaptation to the boundary of the secondary jet and to shock waves.

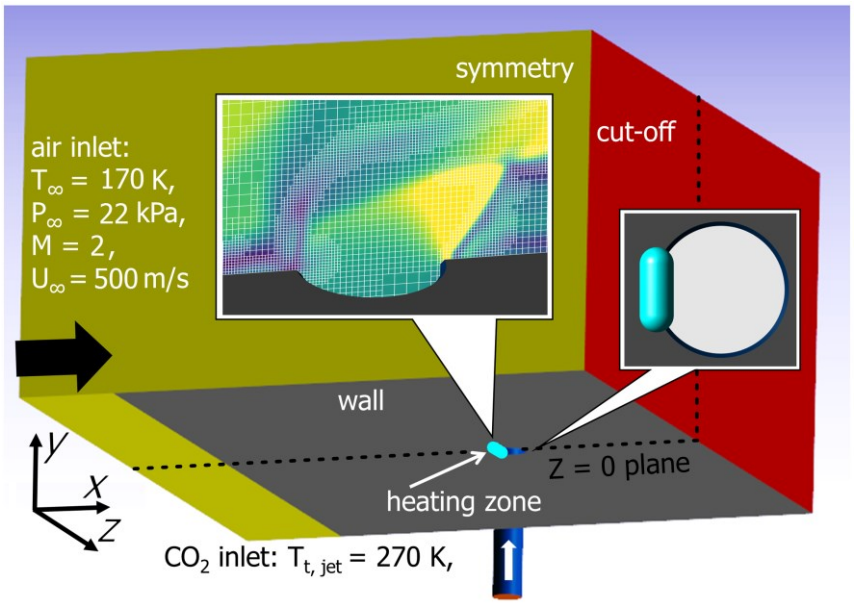

Fig 4. Boundary conditions, computational grid, location of the discharge

The dimensions of the computational domain were chosen for reasons of compliance with the possible conditions of a full-scale experiment on the IADT-50. The supersonic path is 72 mm width (36 mm half-width), 35 mm height and 50 mm length. The injector has a shape of a cylinder 15 mm long and 3 mm in diameter. The center of the injector orifice is taken as the origin. The discharge area has a shape of rounded cylinder with length 2.2 mm and diameter 0.8 mm. On the left side, a uniform input supersonic air flow is specified (black arrow). The input flow parameters correspond to the operating mode of the IADT-50 wind tunnel: velocity 500 m/s, temperature 170 K, pressure 22 kPa.

In our model the injector has the shape of a cylindrical tube due to the features of the planned experiment. CO_2 (white arrow) is used as the secondary jet gas, since in the first experiments this non-flammable gas will be used as a surrogate substance in order to imitate the gaseous fuel. The total gas temperature is 270 K, the mass flow rate Q_m is set 2, 3, 4 g/s (these numbers corresponds to the flow rate in both half-spaces, Z < 0 and Z > 0). The jet-to-crossflow momentum flux ratio J is 0.7, 1.0 and 1.3 corresponding to three mass flow rates.

$$J = \frac{(\rho U^2)_{jet}}{(\rho U^2)_\infty} \quad (1)$$

On the bottom surface (highlighted in grey) and on the wall of the secondary jet injector tube (blue) there is a no-slip boundary condition with standard FlowVision equilibrium wall functions. A small section of the bottom surface at the entrance to the computational domain has a slip boundary condition. On the right wall (highlighted in red) a cut-off boundary condition is set. Slip boundary condition is specified on the remaining surfaces, since, as the calculation in the auxiliary model showed, the side walls have practically no effect on the phenomenon under study.

The computational grid had automatic adaptations to the shocks and to the gradient of CO_2 concentration. The minimal size of computational grid cell was 0.065 mm. The average number of cells was approximately 800,000.

2.4. Spark discharge and simulation of heated medium

The electric discharge is modeled by a volumetric heat source. This approach was previously successfully applied [14] for the simulation of the influence of discharges on gas flows. The volume for heat release is localized at the edge of the injector on the windward side, at the place indicated in the callout in Fig. 4. In the series of calculations presented in this paper, the time-average power of energy release in the spark discharge region is uniform for all the cases: 1 kW (accordingly, 500 W for the simulated subspace Z > 0). The frequency of the spark discharge was varied, and the energy released in one spark was adjusted accordingly. The parameters of energy release in a spark discharge are presented in Table. 1.

Due to the spark discharge the medium can heat up to temperatures over ~ 10,000 K. Therefore our calculations took into account the temperature dependences of the transport coefficients of two media: air [15] and CO_2 [16]. In the cited papers, the transport coefficients were calculated in the temperature range up to 30,000 K for the air medium (gaseous air and equilibrium plasma in the air) and for the Martian atmosphere, which consists almost entirely of CO_2. For a mixture of gases, the transport coefficients in our calculations were determined by molar weighing.

During the heat pulses the time step was 10 ns. After the pulse the step was gradually increased to 100 ns, which correspond to Courant-Friedrichs-Lewy number about 2.

Table 1. Modes of the heat release

Mode	W (mJ)	T (μs)	F (kHz)	Sr
I	100	2	10	0.06
II	50	2	20	0.12
III	33	2	30	0.18
IV	25	2	40	0.24
V	20	2	50	0.30
VI	17	2	60	0.36

3. Results and discussion

The evolution of local characteristics of the JISC flow was calculated for three jet-to-crossflow momentum flux ratios: 0.7, 1.0, 1.3. Local characteristics were obtained for the cases of the absence and presence of periodic spark discharges (heating pulses) with six different modes from Table 1.

Fig. 5 shows the mass fraction of CO_2 in the Z = 0 plane for three J values without spark discharges. Perturbations propagating along the flow (from left to right) are quasiperiodic and, apparently, are caused by absolute instability rather than convective instability, since the geometry of our computational domain minimizes the effect of turbulent boundary layer on JISC flow.

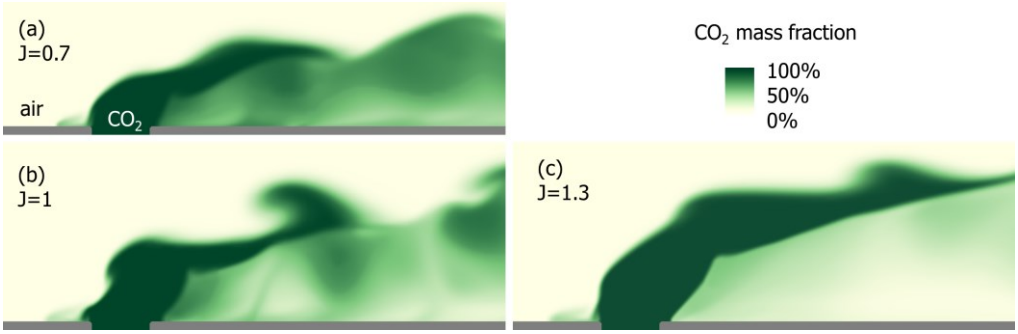

Fig 5. Mass fraction of CO_2 in the absence of pulse heating. View in the Z = 0 plane

Fig. 6 shows the pressure distribution in the Z = 0 and Y = 0 planes before and after the start of a heating pulse. The case shown is calculated with J = 1 and pulsed heating mode IV (40 kHz). The white line shows the conventional boundary of the secondary jet, drawn at the level of 50% CO_2 mass fraction. The diagonal white arrows indicate one large perturbation to make it easy to track.

The set of frames in Fig. 6 demonstrates the shock wave propagation from the heating zone. Propagation is anisotropic due to the fact that in the JISC flow there are both regions of supersonic and subsonic flow. Fig. 6 (d) shows the place where the boundary of the jet bends after the passage of the shock wave. This figure demonstrates the fact that the formation of perturbations in the jet shear layer synchronizes with the spark discharges.

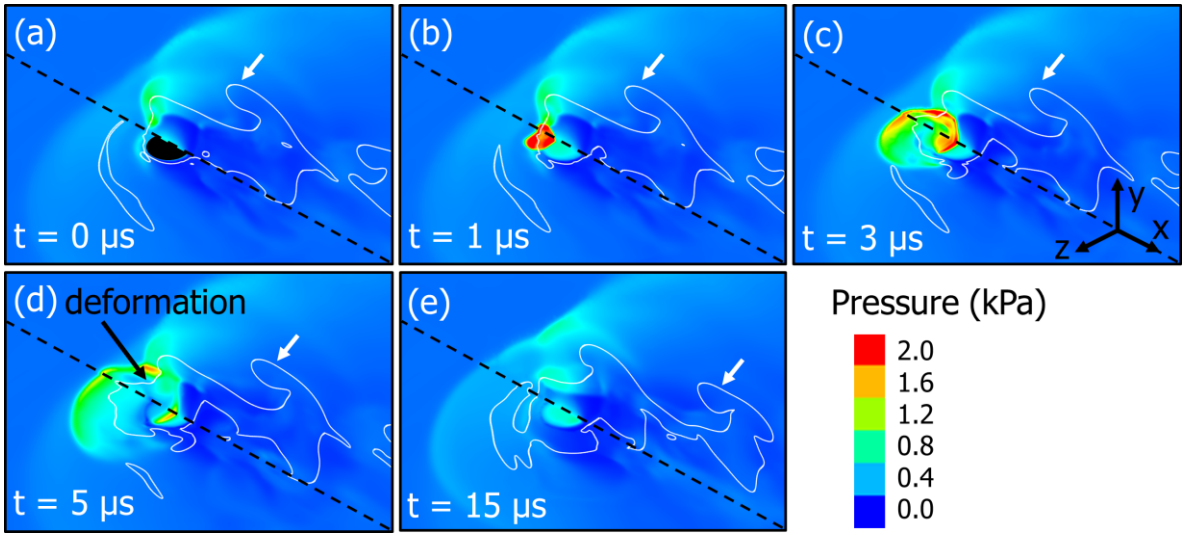

Fig 6. Pressure in the Z = 0 and Y = 0 planes before and after the start of the next heat release pulse. The time t starts from the beginning of one of the heating pulses. The white line indicates the boundary of the secondary jet (50% CO_2 mass fraction). The black semicircle (a) shows the injector orifice

To quantitatively analyze the effect of spark discharges on mixing, the integral criterion of mixing efficiency was used:

$$\eta_m = \frac{\int W_r \rho U \, dA}{\int W \rho U \, dA}, \quad W_r = \begin{cases} W, & W \le W_{st} \\ W_{st} \cdot \left(\frac{1-W}{1-W_{st}}\right), & W > W_{st} \end{cases} \tag{2}$$

where W_{st} is the stoichiometric coefficient. In this work W_{st} is set equal to 0.5, because a non-reacting mixture of air and CO_2 is considered. According to the reasoning given in [17], in our work the instantaneous value of the η_m is calculated and then its average value is calculated.

Fig. 7 shows an example of a time dependence of the instant mixing efficiency for the case with J = 1 and pulsed heating mode VI (60 kHz). Here and below, the integrals in (2) are assumed to be taken over the plane X/D = 5. The presented dependence is quasiperiodic with the frequency equal to the frequency of the spark discharge.

Graphs in Fig. 8 show the dependence of the average value of the integral mixing efficiency for three values of J in the absence of heating (0 kHz) and at 6 different heating frequencies (Table 1).

$$Sr = \frac{F \cdot D}{U_\infty} \tag{3}$$

The error given for the case of J = 1.3, Sr = 0.36 is calculated as the spread of average values of η_m obtained by averaging the instantaneous mixing efficiency (Fig. 7) over several periods. For the remaining cases under study, the error is of the same order of magnitude.

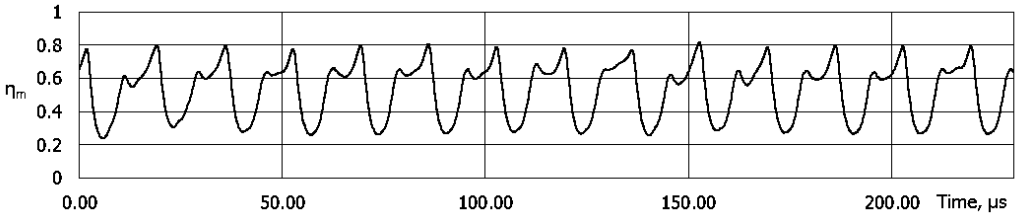

Fig 7. Mixing efficiency in the X/D = 5 plane for the case with J = 1 and heating mode VI (60 kHz)

For all of three J values the maximum of the average mixing efficiency was found at F = 40 kHz. Also for J = 0.7 (which corresponds to the lowest gas flow rate of the secondary jet), the maximum mixing efficiency was achieved at F = 10 kHz.

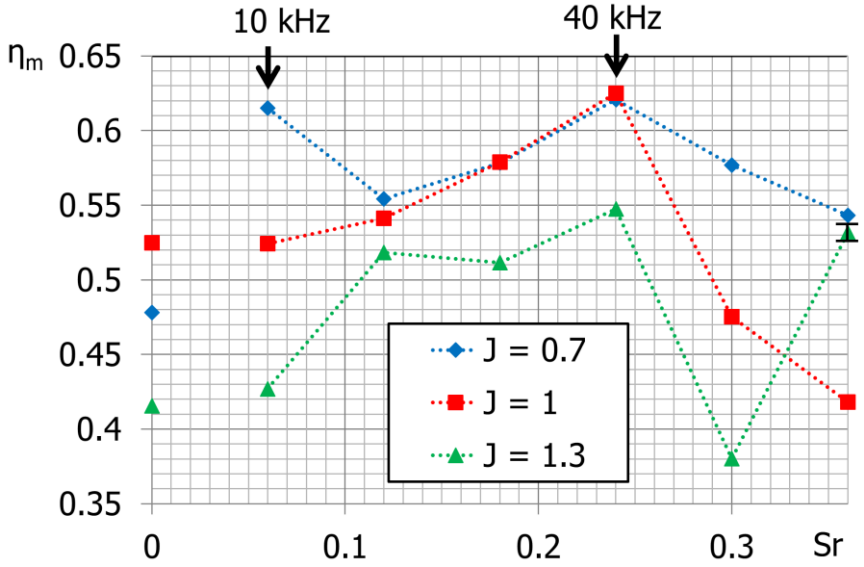

Fig 8. Mixing efficiency dependence on the pulse heating frequency (in terms of Sr) at a constant average energy power. The points are connected for ease of perception

Fig. 9 shows the fields of the CO_2 mass fraction and the temperature for J = 1 in mode IV with F = 40 kHz, as well as modes with F = 30 kHz (mode III) and 50 kHz (mode V). The instantaneous distribution of characteristics is shown for the time step at 10 μs after the beginning of a heat pulse.

Large disturbances emanating from the orifice after pulsed heating can be tracked by the shape of the bend of the secondary jet or by the movement of hot gas portion propagating along the flow. The arrows mark the distance between the center of the injector orifice and the next large disturbance formed as a result of the previous heat release pulse. Note that the distances shown in Fig. 9, are inversely proportional to heating frequencies.

This indicates that, within certain limits, using spark discharges allow one to change the frequency of formation of disturbances in the shear layer on the windward side of the jet and synchronize the formation of disturbances with heat release pulses. This result agrees with the observation outlined in [9].

Probably, the maximum at a frequency of 40 kHz has a resonant nature. The characteristic frequency of the formation of large perturbations in the boundary layer on the windward side of the jet in the

absence of a spark discharge (Fig. 5) is approximately 40 kHz. We suppose that the maximum at F = 40 kHz is conditioned by the following. The spark discharges are synchronized with disturbances that are formed due to absolute instability, therefore the magnitude of perturbations which may arise due to the absolute instability tend to increase at the presence of the discharges. The increase which leads to an acceleration of mixing.

The maximum at F = 10 kHz (Sr = 0.06) for J = 0.7 may probably be conditioned by a qualitative change in the shape of the jet under the influence of a powerful heat pulse. Fig. 10 shows the distribution of the mass fraction of CO_2 for J = 0.7 in the absence of heating (Fig. 10 a), and at two

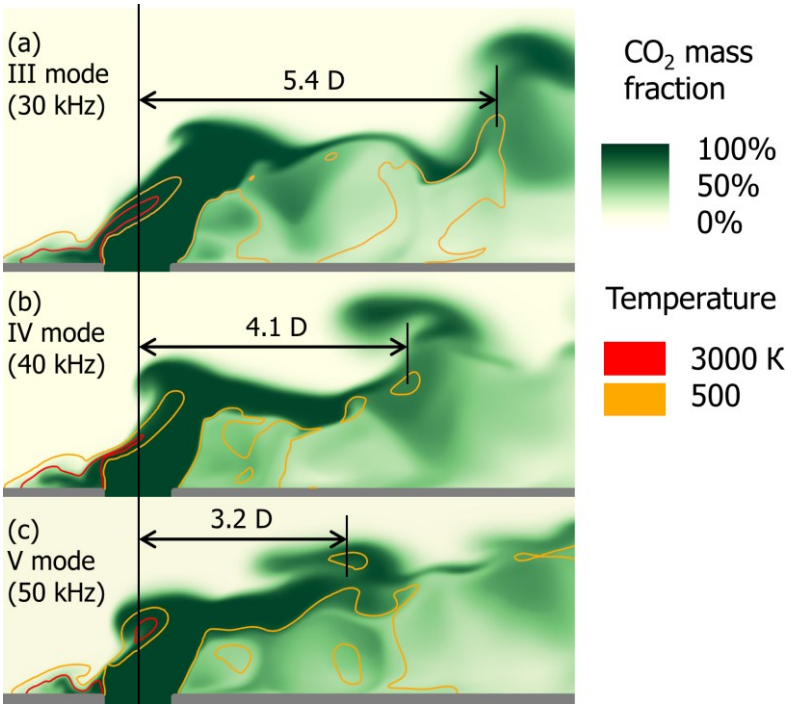

Fig 9. Synchronization of the formation of large perturbations at the jet boundary with heat release pulses. Example for J = 1 with several heating modes. All of the presented fields correspond to time 10 μs after the start of a pulse of heating

Fig 10.

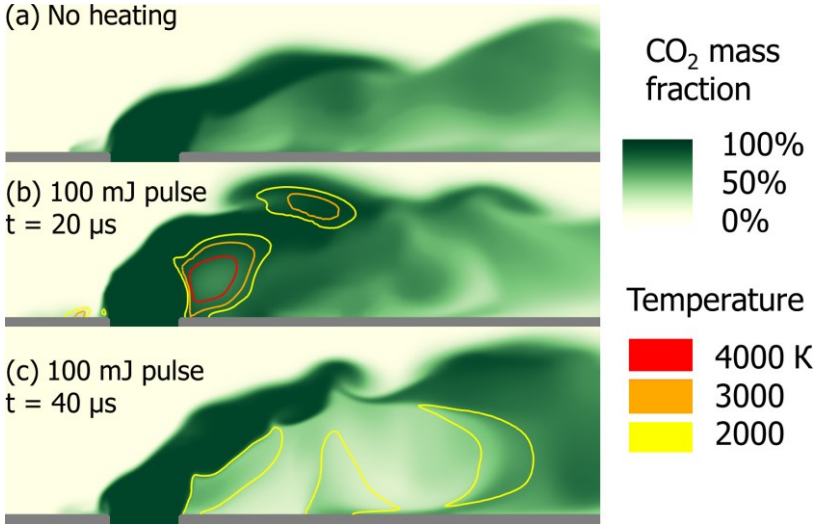

Fig 11. Qualitative temporary change in the shape of the secondary jet under the influence of a powerful spark discharge with energy of 100 mJ (mode I). Mass fraction of CO_2 in the absence of heating (a), 20 μs (b) and 40 μs (c) after the start of heat release. Coloured lines indicate the contours of the temperature field

points in time after the next pulse heating in mode I (Fig. 10 b, c). In the absence of heating, the CO_2 jet propagates downstream predominantly near the injection surface. A powerful discharge makes it possible to increase the depth of penetration of the jet, and this effect lasts 40 μs or more, that is, about half the time interval between discharges. This is possibly the reason of reaching a maximum of mixing efficiency.

It is notable that for J = 1 and J = 1.3 in some heating modes the mixing efficiency decreases compared to the case of no heating (Fig. 8). The reason for this is probably the fact that the disturbance from the spark discharge in these modes prevents the formation of disturbances caused by absolute instability.

The average released power (1 kW) was about 1% of a power of complete ethylene fuel combustion with the same mass flow as the CO_2 mass flow in our calculations. Nevertheless, the mixing efficiency in some cases (Fig. 8) was increased by up to 15% due to the pulsed energy deposition via spark discharges.

4. Conclusion

By the FlowVision software package, using the URANS method with the KEFV turbulence model, the evolution of the JISC flow characteristics was calculated in the absence and presence of a periodic spark discharges near the windward edge of the injector orifice. The impact of the discharge on its environment was modeled using local pulse-periodic heat release in the area of discharge localization.

For several values of J and several modes of pulsed heat release (Table 1), we obtained the time-averaged value of the η_m integral criterion for mixing efficiency in a certain plane. For several special cases corresponding to maxima of mixing efficiency, the possible reasons for the existence of these maxima were qualitatively considered.

The presented series of calculations serve to preparation for full-scale experiments in the IADT-50 wind tunnel in Joint Institute for High Temperatures of the Russian Academy of Sciences. In the experiments the effect of periodic spark discharges on the JISC flow will be investigated.

Acknowledgements

The work was supported by the Russian Science Foundation grant No. 21-79-10408.

References

1. A.A., Savelkin, K.V., Yarantsev, D.A., Leonov, S.B.: Plasma-enhanced mixing and flameholding insupersonic flow. Phil. Trans. R. Soc. A (2015). https://doi.org/10.1098/rsta.2014.0337
2. Liu, Q., Baccarella, D., & Lee, T.: Review of combustion stabilization for hypersonic airbreathing propulsion. Progress in Aerospace Sciences (2020). https://doi.org/10.1016/j.paerosci.2020.100636
3. Cai, Z., Gao, F., Wang, H., Ma, C., Yang, T.: Numerical Study on Transverse Jet Mixing Enhanced by High Frequency Energy Deposition. Energies (2022). https://doi.org/10.3390/en15218264
4. Liu, X., Sun, M., Li, P., Li, F., Wang, C., Yang, X., Wang, H., Yang, Y., Xiong, D., Wang, Y.: Effect of kerosene injection states on mixing and combustion characteristics in supersonic combustor at high equivalent ratio. Phys. Fluids (2024). https://doi.org/10.1063/5.0177046
5. Chen, J., Sun, M., Li, P., An, B., Jiaoru, W., Li, M.: Effect of kerosene injection states on mixing and combustion characteristics in supersonic combustor at high equivalent ratio. Phys. Fluids (2024). https://doi.org/10.1063/5.0177046
6. Liu, M., Sun, M., Yang, D., Zhao, G., Tang, T., An, B., Wang, H.: Mixing and combustion characteristics in a scramjet combustor with different distances between cavity and backward facing step. Chinese Journal of Aeronautics (2023). https://doi.org/10.1016/j.cja.2023.04.013

7. Li, F., Li, P., Liu, X., Wang, H., Sun, M., Wang, Z.: Numerical study on the mixing and combustion characteristics of a liquid kerosene jet in a scramjet combustor. Aerospace Science and Technology (2023). https://doi.org/10.1016/j.ast.2023.108362
8. Zhou, Y., Cai, Z., Li, Q., Li, C., Sun, M., Gong, S.: Spray characteristics of a liquid fuel jet in a tandem backward-facing step cavity in supersonic flow. Aerospace Science and Technology (2023). https://doi.org/10.1016/j.ast.2023.108514
9. Volkov, L.S., Firsov, A.A.: Modeling the influence of repetitively pulsed heating on the formation of perturbations at the boundary of a transverse jet in a supersonic crossflow. Computer Research and Modeling (2023). https://doi.org/10.20537/2076-7633-2023-15-4-845-860
10. Zhluktov, S.V., Aksenov, A.A.: Wall functions for high-Reynolds calculations in FlowVision software. Computer Research and Modeling (2015). https://doi.org/10.20537/2076-7633-2015-7-6-1221-1239
11. Santiago, J.G., Dutton, J.C.: Velocity measurements of a jet injected into a supersonic crossflow. J. Propuls Power (1997). https://doi.org/10.2514/2.5158
12. Kawai, S., Lele, S.K. Large-eddy simulation of jet mixing in supersonic crossflows. AIAA Journal (2010). https://doi.org/10.2514/1.J050282
13. Rasheed, I., Mishra, D.P.: Numerical study of a sonic jet in a supersonic crossflow over a flat plate. Physics of Fluids (2020). https://doi.org/10.1063/5.0026214
14. Dolgov, E.V., Kolosov, N.S., Firsov, A.A. The study of the discharge influence on mixing of gaseous fuel jet with the supersonic air flow. Computer Research and Modeling (2019). https://doi.org/10.20537/2076-7633-2019-11-5-849-860
15. Capitelli, M., Colonna, G., Gorse, C., D'angola, A. Transport properties of high temperature air in local thermodynamic equilibrium. The European Physical Journal D (2000). https://doi.org/10.1007/s100530070094
16. Catalfamo, C., Bruno, D, Colonna, G., Laricchiuta, A., Capitelli, M. High temperature Mars atmosphere. Part II: Transport properties. The European Physical Journal D (2009). https://doi.org/10.1140/epjd/e2009-00193-6
17. Watanabe, J., Kouchi, T., Takita, K., Masuya, G.: Large-eddy simulation of jet in supersonic crossflow with different injectant species. AIAA Journal (2012). https://doi.org/10.2514/1.J051550